Proceedings of the 1998 IEEE/RSJ
Intl. Conference on Intelligent Robots and Systems
Victoria, B.C., Canada • October 1998

The Motion Isotropy Hypersurface: A Characterization of Acceleration Capability

Alan Bowling and Oussama Khatib

Robotics Laboratory
Computer Science Department
Stanford University
Stanford, CA, USA 94305

Abstract

The study of acceleration capability is concerned with the responsiveness of a manipulator to controller commands. In this paper we present a general model for the analysis of end-effector linear and angular accelerations that accounts for the velocity effects. The separate treatment of linear and angular motion directly addresses the inhomogeneities of end-effector motions, avoiding the use of indeterminate scaling factors. The velocity effects considered are the Coriolis and centrifugal forces, as well as the relationships associated with actuator's speed-torque performance curves. This study results in a characterization referred to as the "motion isotropy hypersurface" which describes the relationships between isotropic end-effector linear and angular velocities and accelerations. The utility of this surface and its associated information is demonstrated in a design application involving the PUMA 560 manipulator.

1 Introduction

In recent years, various models have been proposed for the analysis of manipulator performance. The aim of these models is to provide a characterization of the responsiveness of of a manipulator in the execution of a task. Our approach to addressing this problem is to analyze the relationships between the end-effector linear and angular accelerations and velocities, $\dot{v}$, $\dot{\omega}$, v, and ω; Figure 1. Note that these are directional quantities. When analyzing mechanisms intended for general tasks it is necessary to consider its capabilities in all directions, and therefore these quantities are explored in terms of their isotropic magnitudes.

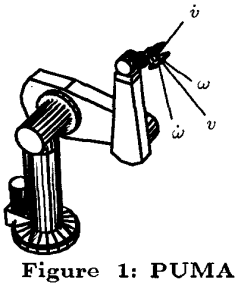

Figure 1: PUMA

In earlier work, both the kinematic and dynamic aspects of this problem have been considered. The kinematic studies focused on the analysis of the Jacobian matrix. Proposed kinematic measures include the Jacobian condition number [10, 16], manipulability measure [18, 20], and norm of the Jacobian rate of change [15]. In dynamic analyses, the proposed measures and characterizations include the generalized inertia ellipsoid [1], the end-effector mass matrix [6], dynamic manipulability ellipsoid [19, 21], dynamic conditioning index [12], acceleration set theory [8, 9], isotropic acceleration radius [5], acceleration hyperparallelipiped [7], and other measures discussed in [11, 13, 14, 22]. Thomas, Yuan-Chow, and Tesar [17] come the closest to the treatment presented here. However, a common difficulty encountered in these studies is the treatment of the inhomogeneities between linear and angular motions. This difficulty is often addressed by the introduction of scaling factors.

Our earlier studies of end-effector motion [3, 4] resulted in a characterization of end-effector acceleration capability referred to as the *motion isotropy hypersurface*. In this paper, we extend these analyses with a comprehensive treatment of linear and angular velocities. This treatment includes the effects of the actuator's speed-torque performance curve, which describes the reduction of torque capacity due to rotor velocity.

This study of isotropic properties provides a "worst case" characterization of achievable velocities and accelerations. These worst-case motions are described by

the motion isotropy hypersurface and the information obtained from its development. This article presents the development of the hypersurface and its associated information, for non-redundant manipulators. The utility of this analysis is demonstrated through a design application involving the PUMA 560 manipulator.

2 Model

In this section the equations describing the motion isotropy hypersurface for a non-redundant manipulator are developed. A more extensive discussion is presented in [2]. The development begins with the familiar joint space equations of motion

$$A\,\ddot{\mathbf{q}} + \mathbf{b} + \mathbf{g} = \mathbf{\Gamma} = \mathsf{G}\,\mathbf{\Upsilon}. \tag{1}$$

where $\mathbf{q}$, A, $\mathbf{b}$, $\mathbf{g}$, $\mathbf{\Gamma}$, $\mathbf{\Upsilon}$, and G, represent the n joint coordinates, joint space kinetic energy matrix, centrifugal and Coriolis forces, gravity forces, joint torques and forces, actuator torques produced between the rotor and stator, and transformation between actuator and joint torques.

The goal is to transform equation (1) into a set of inequalities relating the actuator torque capacities to end-effector accelerations. This is accomplished using the Jacobian, J, defined as

$$\boldsymbol{\vartheta} \triangleq \begin{bmatrix} \boldsymbol{v} \\ \boldsymbol{\omega} \end{bmatrix} = J\,\dot{\mathbf{q}} \tag{2}$$

where $\boldsymbol{v}$ and $\boldsymbol{\omega}$ are end-effector linear and angular velocities. Just as joint torques are related to actuator torques, joint speeds are related to actuator, or rotor, speeds as follows

$$\dot{\boldsymbol{\theta}} = \mathsf{G}^T\,\dot{\mathbf{q}} = \mathsf{G}^T\,J^{-1}\,\boldsymbol{\vartheta} \tag{3}$$

where $\dot{\boldsymbol{\theta}}$ is the vector of n rotor speeds. The bound on actuator torque capacity can be expressed as;

$$|\Upsilon_i| \le \Upsilon_{bound_i}(\dot{\theta}_i, \ldots). \tag{4}$$

Ideally Υ_{bound_i} is a linear function of rotor velocity referred to as the *speed-torque curve*, Figure 2. However, using this linear function complicates the velocity analysis, so the speed-torque curve is approximated by a second order function without a linear term, Figure 2. This choice is made because the actual speed-torque curve may be nonlinear. The final model has the form

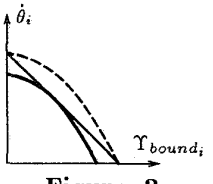

Figure 2: Speed-Torque Curve

$$\Upsilon_{bound_i} = {}_0\Upsilon_i - {}_2\Upsilon_{iii}\,\dot{\theta}_i^2 \tag{5}$$

where ${}_0\Upsilon_i$ is usually the peak torque and ${}_2\Upsilon_{iii}$ is a scalar used to approximate the slope of the speed-torque curve. It is expressed as an element of a third order tensor where all elements other than the iii^{th} are zero. Equation (4) can be expressed in terms of an upper and lower bound using equation (5)

$$-{}_0\Upsilon_i - \mathsf{b}(x)\,{}_2\Upsilon_{iii}\,\dot{\theta}_i^2 \le \Upsilon_i \le {}_0\Upsilon_i - \mathsf{b}(x)\,{}_2\Upsilon_{iii}\,\dot{\theta}_i^2 \tag{6}$$

where $\mathsf{b}(x)$ equals positive or negative one depending on the boundary of interest

$$\mathsf{b}(x) = \begin{cases} 1 & \text{if} \quad x = upper \\ -1 & \text{if} \quad x = lower \end{cases}. \tag{7}$$

These bounds are normalized and expressed in terms of end-effector velocities using equation (3) to obtain

$$-\mathbf{1} \le N(\,\mathbf{\Upsilon} + \mathsf{b}(x)\mathbf{t}\,) \le \mathbf{1} \tag{8}$$

where $\mathbf{1}$ is a vector of ones and

$$\mathbf{t} = \begin{bmatrix} \boldsymbol{\vartheta}^T \mathsf{T}_1 \boldsymbol{\vartheta} \\ \vdots \\ \boldsymbol{\vartheta}^T \mathsf{T}_n \boldsymbol{\vartheta} \end{bmatrix} = N \begin{bmatrix} \boldsymbol{\vartheta}^T J^{-T} \mathsf{G}\,{}_2\Upsilon_1\,\mathsf{G}^T J^{-1}\boldsymbol{\vartheta} \\ \vdots \\ \boldsymbol{\vartheta}^T J^{-T} \mathsf{G}\,{}_2\Upsilon_n\,\mathsf{G}^T J^{-1}\boldsymbol{\vartheta} \end{bmatrix} \tag{9}$$

where N is a diagonal matrix where $N_{ii} = \frac{1}{{}_0\Upsilon_i}$.

Omitting the details, equations (1), (2), and (9) can be used to obtain

$$\boxed{\mathbf{\Upsilon}_{lower} \le E_v \dot{\boldsymbol{v}} + E_\omega \dot{\boldsymbol{\omega}} + \mathbf{h} \le \mathbf{\Upsilon}_{upper}} \tag{10}$$

where

$$\begin{aligned}
[\,E_v\;E_\omega\,] &= E = N\mathsf{G}^{-1}AJ^{-1} \\
\begin{bmatrix} \dot{\mathbf{q}}^T B_1 \dot{\mathbf{q}} \\ \vdots \\ \dot{\mathbf{q}}^T B_n \dot{\mathbf{q}} \end{bmatrix} &= \mathbf{b} - AJ^{-1}\dot{J}\dot{\mathbf{q}} \\
\begin{bmatrix} \boldsymbol{\vartheta}^T M_1 \boldsymbol{\vartheta} \\ \vdots \\ \boldsymbol{\vartheta}^T M_a \boldsymbol{\vartheta} \end{bmatrix} &= N\mathsf{G}^{-1} \begin{bmatrix} \boldsymbol{\vartheta}^T J^{-T} B_1 J^{-1} \boldsymbol{\vartheta} \\ \vdots \\ \boldsymbol{\vartheta}^T J^{-T} B_n J^{-1} \boldsymbol{\vartheta} \end{bmatrix} \\
\mathbf{h} = \begin{bmatrix} \boldsymbol{\vartheta}^T \mathrm{H}_1 \boldsymbol{\vartheta} \\ \vdots \\ \boldsymbol{\vartheta}^T \mathrm{H}_a \boldsymbol{\vartheta} \end{bmatrix} &= \begin{bmatrix} \boldsymbol{\vartheta}^T M_1 \boldsymbol{\vartheta} \\ \vdots \\ \boldsymbol{\vartheta}^T M_a \boldsymbol{\vartheta} \end{bmatrix} + \mathsf{b}(x)\mathbf{t} \\
\mathbf{\Upsilon}_{upper} &= N\left(\,{}_0\mathbf{\Upsilon} - \mathsf{G}^{-1}\,\mathbf{g}\,\right) \\
\mathbf{\Upsilon}_{lower} &= -N\left(\,{}_0\mathbf{\Upsilon} + \mathsf{G}^{-1}\,\mathbf{g}\,\right).
\end{aligned} \tag{11}$$

The separation of linear and angular characteristics in equation (10) is motivated by the need to analyze these properties separately.

3 Isotropy Equations

Geometric and algebraic approaches are used to analyze equation (10). In the geometric approach each term is represented by a geometric object and the relationship between them is explored [3, 4]. Insights obtained from the geometric approach facilitate the development of the algebraic approach which is more useful for analyzing velocities.

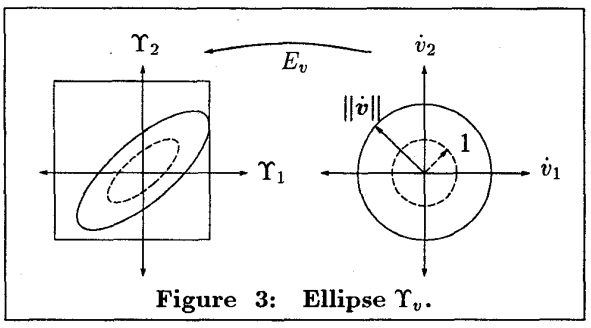

Figure 3: Ellipse Υ_v.

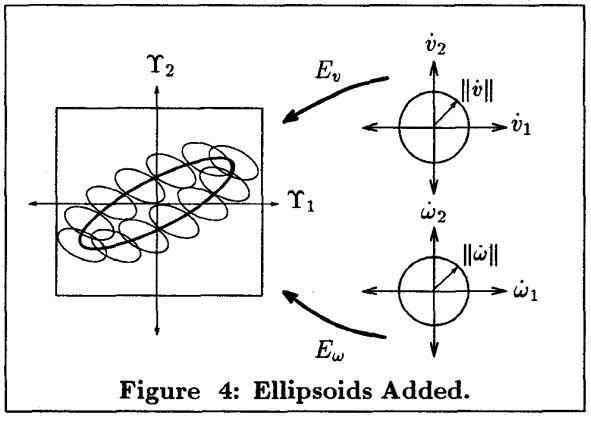

Figure 4: Ellipsoids Added.

In the geometric approach, the torque bounds are interpreted as an n-dimensional hypercube, the square in Figure 3, whose center is shifted away from the origin by the gravity effect, i.e. $N\mathsf{G}^{-1}\mathbf{g}$ in equation (11). Now consider the linear acceleration term in equation (10), $E_v\dot{v}$. Motions are interpreted as isotropic quantities represented by spheres

$$\dot{v}^T\dot{v} \;=\; \|\dot{v}\|^2. \tag{12}$$

This sphere is transformed by E_v into an ellipsoid in torque space using the following relationship

$$\dot{v} = E_v^+\ \Upsilon_v \tag{13}$$

where E_v^+ is the left inverse of E_v. Equations (12) and (13) are used to obtain the ellipsoid

$$\Upsilon_v^T(E_vE_v^T)^+\Upsilon_v = \|\dot{v}\|^2. \tag{14}$$

The isotropic acceleration is determined by expanding the ellipsoid until it is inscribed within the bounds, Figure 3. Note that only the vectors associated with the tangency points, referred to as *tangency vectors*, need to be examined. The ellipsoids seldom align with the coordinate axes, making it difficult to realistically illustrate the geometric approach. However, although unrealistic, these figures still represent valid concepts.

A similar process is followed to obtain the torque ellipsoid representing angular accelerations

$$\Upsilon_\omega^T(E_\omega E_\omega^T)^+\Upsilon_\omega \;=\; \|\dot{\omega}\|^2. \tag{15}$$

All possible sums of the vectors Υ_v and Υ_ω are considered by mapping the center of one ellipsoid onto every point on the surface of the other, Figure 4. Corresponding tangency vectors from each ellipsoid are added to obtain the resultant which touches a particular bound, Figure 5.

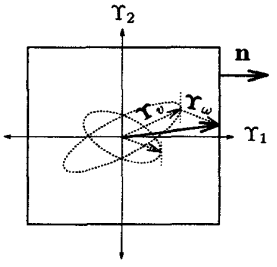

Figure 5: Tangency Vectors

The resultant vector touching the boundary in Figure 5 must satisfy

$$\mathbf{n}\cdot(\ \Upsilon_v + \Upsilon_\omega\ ) = \Upsilon_{upper_1} \tag{16}$$

where $\mathbf{n}$ is normal to the boundary plane 1 as shown Figure 5. If the vectors $\overline{\Upsilon}_v$ and $\overline{\Upsilon}_\omega$ are defined as,

$$\overline{\Upsilon}_v^T(E_vE_v^T)^+\overline{\Upsilon}_v = 1 \quad \overline{\Upsilon}_\omega^T(E_\omega E_\omega^T)^+\overline{\Upsilon}_\omega = 1 \tag{17}$$

(the dashed ellipse in Figure 3), Υ_v and Υ_ω can be expressed in terms of these vectors in order to obtain

$$\mathbf{n}\cdot(\ \|\dot{v}\|\overline{\Upsilon}_v + \|\dot{\omega}\|\overline{\Upsilon}_\omega\ ) = \Upsilon_{upper_1}. \tag{18}$$

Equation (18) represents a line with respect to $\|\dot{v}\|$ and $\|\dot{\omega}\|$. $2n$ relations similar to equation (18) are obtained for each boundary plane. The isotropic accelerations are determined by the most limiting relationship(s) from the set. Determining the line(s) which represent the most limiting relationships corresponds to finding the innermost envelope formed around the origin when the $2n$ lines are overlayed in the same space.

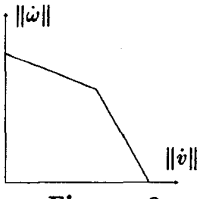

Figure 6: Isotropy Curve

This curve is convex and piecewise linear, shown in Figure 6. A discontinuity in the curve occurs when the limiting boundary changes.

The geometric approach does not work well for the velocity dependent terms, because they cannot be separated into linear and angular subspaces. In addition, the torque surface corresponding to the isotropic velocity surfaces is difficult to determine because the velocity dependent terms are second order. However, equation (18) shows that only the component of the tangency vector in the direction of its associated boundary is important. These components, $\mathbf{n} \cdot \overline{\Upsilon}_v$ and $\mathbf{n} \cdot \overline{\Upsilon}_\omega$, can be expressed succinctly as

$$\mathbb{A} \left[\, \|\dot{v}\| \;\; \|\dot{\omega}\| \, \right]^T \;=\; \mathbb{T} \tag{19}$$

where $\mathbb{A}$ is a $2n \times 2$ matrix containing the aforementioned components and $\mathbb{T}$ contains the elements of Υ_{upper} and Υ_{lower}. The goal is to determine the corresponding components from the velocity dependent terms. Doing this requires a more algebraic approach. This approach will first be presented in terms of acceleration since this facilitates consideration of velocities.

Of the vectors comprising an ellipsoid, the tangency vector has the largest component in the direction of its associated boundary. For accelerations, the components of the vectors comprising the ellipsoid in the direction of the i^{th} actuator are determined by the i^{th} row of the E matrix, equation (11). The largest/smallest value of this component, which is the tangency vector component, can be found as follows:

$$\begin{aligned} \text{minimize/maximize} \quad & \Upsilon_i = \left[\, E_{i1} \cdots E_{in} \, \right] \begin{bmatrix} \dot{v} \\ \dot{\omega} \end{bmatrix} \\ \text{subject to} \quad & \dot{v}^T \dot{v} = \|\dot{v}\|^2 \qquad \dot{\omega}^T \dot{\omega} = \|\dot{\omega}\|^2. \end{aligned} \tag{20}$$

This system is maximized, for the upper bound, or minimized, for the lower bound, with respect to $\dot{v}$ and $\dot{\omega}$ yielding a solution expressed in terms of $\|\dot{v}\|$ and $\|\dot{\omega}\|$. Applying the method of Lagrange multipliers to this system yields an easily solvable eigenvalue problem where the elements of $\mathbb{A}$ can be defined as

$$\begin{aligned} \mathbb{A}_{2j-1,1} \;=\; \mathbb{A}_{2j,1} \;&=\; +\sqrt{\sum_{k=1}^{p} E_{jk}^2} \\ \mathbb{A}_{2j-1,2} \;=\; \mathbb{A}_{2j,2} \;&=\; +\sqrt{\sum_{k=p+1}^{n} E_{jk}^2} \end{aligned} \tag{21}$$

where $j = (1, \ldots, n)$, v has dimension p, and ω has dimension $r = n - p$.

When considering velocities, the component of the tangency vector in the direction of i^{th} actuator torque boundary is determined by the i^{th} quadratic term in the $\mathbf{h}$ vector;

$$\begin{aligned} \text{minimize/maximize} \quad & \Upsilon_i = \vartheta^T H_i \vartheta \\ \text{subject to} \quad & \dot{v}^T \dot{v} = \|\dot{v}\|^2 \qquad \dot{\omega}^T \dot{\omega} = \|\dot{\omega}\|^2. \end{aligned} \tag{22}$$

Recall that when considering the upper bound, $H_i = M_i + \mathsf{b}(upper)\mathsf{T}_i$ (and similarly for the lower bound). For this system, it is very difficult to find a closed form analytical solution, in terms of $\|\dot{v}\|$ and $\|\dot{\omega}\|$. However, a useful partial solution can be found, which will be discussed momentarily. This solution can be included in equation (19) as $\mathbb{C}$,

$$\boxed{\mathbb{A} \left[\, \|\dot{v}\| \;\; \|\dot{\omega}\| \, \right]^T + \mathbb{C} \left(\, \|v\|, \|\omega\| \, \right) \;=\; \mathbb{T}.} \tag{23}$$

where $\mathbb{C} \left(\, \|v\|, \|\omega\| \, \right)$ is a second order function of $\|v\|$ and $\|\omega\|$. These relations are referred to as the *motion isotropy equations.*

With the addition of the new terms each relation in equation (23) represents a hypersurface in four-space, as opposed to the lines represented by equation (19). Similarly to Figure 6, the motion isotropy hypersurface is determined by the innermost envelope formed by these hyperplanes.

However, a four-dimensional hypersurface is difficult to display, so it must be sectioned by a hyperplane in order to show its characteristics. The sectioning hyperplane is usually chosen as $\|v\| = 0$, $\|\omega\| = 0$, or $\|\omega\| = \eta \|v\|$ (note that the first two sections are special cases of the third where $\eta = 0$ and $\eta = \infty$). This hyperplane is chosen because the useful partial solution for the velocity terms can be obtained with this added constraint on the optimization problem of equation (22). Also, since this hyperplane contains the origin, the resulting section gives a better picture of the volume encompassed by the hypersurface. A description of the full surface can be obtained from the set of surfaces where η is varied from 0 to ∞.

The partial solution for the velocity dependent terms can be obtained as follows. Since the minimization and maximization problems are similar only the former will be discussed. First note that H_i can be made positive semi-definite thereby ensuring the existence of a maximum value. Doing this involves multiplying the constraints by the smallest eigenvalue of H_i, and adding them to Υ_i,

$$\Upsilon_i \;=\; \vartheta^T \overset{shift}{H_i} \vartheta \;+\; \lambda_{min} \left(\, \|v\|^2 + \|\omega\|^2 \, \right) \tag{24}$$

where λ_{min} is a real number since H_i is symmetric. A change of variables is performed,

$$\|\omega\| \;=\; \eta \, \|v\| \tag{25}$$

$$\vartheta = [\, \|v\|\ \overline{v}\ \ \|\omega\|\ \overline{\omega}\,]^T \qquad (26)$$

where η is a positive scalar and $\overline{v}$ and $\overline{\omega}$ are unit vectors, yielding

$$\begin{bmatrix} v \\ \omega \end{bmatrix} = \|v\| \begin{bmatrix} \overline{v} \\ \eta\,\overline{\omega} \end{bmatrix}. \qquad (27)$$

Using equation (27), the problem expressed in equations (22) and (24) is transformed into

$$\Upsilon_i = \|v\|^2 \left(\begin{bmatrix} \overline{v} \\ \eta\,\overline{\omega} \end{bmatrix}^T {}^{shift}H_i \begin{bmatrix} \overline{v} \\ \eta\,\overline{\omega} \end{bmatrix} + \lambda_{min}\,(\,1+\eta^2\,) \right)$$

$$\overline{v}^T\overline{v} = 1 \qquad \overline{\omega}^T\overline{\omega} = 1. \qquad (28)$$

Solving this problem only requires the maximization of the first term in parenthesis with respect to the unit vectors $\overline{v}$ and $\overline{\omega}$, since $\|v\|$ is only a multiplicative factor and the second term can be considered constant.

Still, an analytical solution to this problem is very difficult to find (it does not correspond to any eigenvectors of the matrix involved except in special cases). However, assigning a value to η yields a problem solvable using publicly available search algorithms. The solution has the form

$$\Upsilon_{i_{max}} = c\,\|v\|^2. \qquad (29)$$

These components are added into equation (19) as the vector $\mathbb{C}$ $(\|v\|, \|\omega\|)$ in the motion isotropy equations. The elements of $\mathbb{C}$ can be defined similarly to the elements of $\mathbb{A}$ in equation (21), although the expressions are more complex.

4 Motion Isotropy Hypersurface

The motion isotropy hypersurface describes the bounds on isotropic accelerations and therefore any motions lying beneath it are possible in every direction. An example of the isotropy surface where $\|\omega\| = 0$ is shown in Figure 7a for the PUMA 560 at the configuration shown in Figure 7b. However, the actuators used here are not the original ones shipped with this manipulator. First note that the curve in the $\|\dot{v}\|$-$\|\dot{\omega}\|$ plane is convex, recall Figure 6. Also note that, by equation (29), any section obtained using a hyperplane of the form $\|\omega\| = \eta\|v\|$ is also convex. However, it is difficult to know whether the entire hypersurface is convex.

The hypersurface is physically meaningful, describing the worst case combinations of linear and angular accelerations and velocities which saturate the actuators. The actuator which saturates first is termed the *limiting actuator*. In the example, the motor actuating the first joint of PUMA 560 is the limiting actuator, indicated by the numeric label on the surface of Figure 7a. The resultant tangency vectors for the boundary corresponding to the limiting actuator can be used to determine the combination of motion which saturated that actuator, displayed in Figure 7b. The magnitudes of these worst case motions are described by the hypersurface.

Consider the point marked by the △ in Figure 7a. This point represents the isotropic linear acceleration achievable from rest if the end-effector moves without changing its orientation, $\dot{\omega} = \omega = v = 0$. At △ the actuator of the first joint saturated attempting to provide a linear acceleration of $5.1 m/s^2$ in the direction denoted by $\dot{v}$ in Figure 7b.

The curve in the $\|\dot{v}\|$-$\|\dot{\omega}\|$ plane describes the combinations of isotropic linear and angular acceleration, at zero velocity $\omega = v = 0$, which saturate the first actuator. The intercept along $\|\dot{\omega}\|$ axis, marked by ○, denotes the isotropic angular acceleration achievable from rest if the end-effector rotates without translating the operational point, $48.4 rad/s^2$.

Coming out of the $\|\dot{v}\|$-$\|\dot{\omega}\|$ plane, the bounds on acceleration capability when accelerating from a particular velocity state are displayed. End-effector velocities can limit performance because the manipulator must overcome Coriolis/centrifugal forces while the torque capacities decline in accordance with the speed-torque curve. The shape of the surface shows that the magnitude of acceleration attainable in every direction decreases as the isotropic linear velocity increases. The point marked by □ in Figure 7a marks the magnitude of linear velocity, $1.4 m/s$, where the manipulator cannot provide any arbitrary accelerations because all of the available torque from the limiting actuator is used to compensate for the Coriolis, centrifugal, and gravity forces.

The motion isotropy hypersurface and its contained information can be applied to the manipulator design problems; specifically the actuator selection problem. This involves determining the actuators which will provide a desired level of performance. In this process the motion isotropy hypersurface is used to evaluate a manipulator's current performance. The limiting actuator then indicates which actuator torque to alter in order to improve performance. This information is used within a heuristic algorithm for actuator selection, however the algorithm will not be discussed here. An example of its use is presented to illustrate the utility of the motion isotropy hypersurface and its limiting actuator information.

For example, consider increasing the $\|\dot{v}\|$ intercept

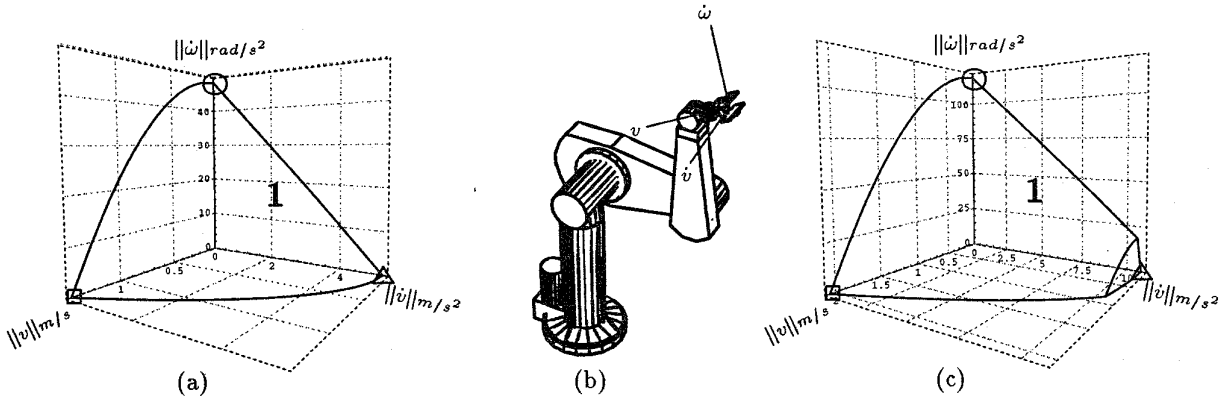

Figure 7: Isotropy Surface

of Figure 7a to $1g$, $9.81 m/s^2$. The requisite actuators are shown in Table 1 and the resulting isotropy surface is shown in Figure 7c. The velocity information for these actuators is given in Table 2, where ${}_2\Upsilon_{iii} = {}_0\Upsilon_i / \dot{\theta}^2_{i_{max}}$.

	Actuator Peak Torque ${}_0\Upsilon_i$ Nm					
Joint	1	2	3	4	5	6
Original	0.65	0.86	0.43	0.22	0.22	0.22
New	1.6	1.23	0.43	0.22	0.22	0.22

Table 1: Actuator Selection

Joint	1	2	3	4	5	6
${}_0\Upsilon_i$ Nm	0.22	0.43	0.65	0.86	1.23	1.60
$\dot{\theta}_{i_{max}}$ rad/s	1885	1414	1204	1079	922	859

Table 2: Actuator Maximum Velocity

Note that improved motion isotropy hypersurface section is comprised of two surface patches which means the limiting actuator changes between the first and third actuators (the label indicating third actuator is omitted from Figure 7c). As expected, it is necessary to increase the first actuator. It is also necessary to increase the second actuator in order to achieve the desired performance, however the heuristic knows to do this based on the limiting actuator information obtained at different stages in the procedure.

Since the hypersurface is four-dimensional it is necessary to develop some measures which summarize its characteristics. These measures also reduce the necessity for actually generating the hypersurface, by summarizing the features discussed above. However, due to space limitations, they will not be presented here. A complete description of them can be found in [2] and will be presented in a later article.

5 Conclusion

The motion isotropy hypersurface presented in this paper provides a characterization of the end-effector isotropic acceleration capabilities at a given configuration. By addressing the inhomogeneity problem, this approach allows full analyses of linear and angular accelerations and velocities. This procedure also yields insights into the limiting actuators, as motor saturation determines the extent of isotropic motions. In addition, the analysis provides information about the directions of acceleration and velocity in which an actuator will saturate. The motion isotropy hypersurface also provides a physically meaningful worst-case analysis of the end-effector motions. These models have been extended to redundant manipulators [4]. The analysis of end-effector force capability can also be included in these models [2].

6 Acknowledgments

The financial support of NASA/JPL, Boeing, Hitachi Construction Machinery, and NSF, grant IRI-9320017, are gratefully acknowledged. Also many thanks to Professor Walter Murray.

References

[1] Haruhiko Asada. A geometrical representation of manipulator dynamics and its application to arm design. *Journal of Dynamic Systems, Measurement, and Control*, 105(3):131–135, September 1983.

[2] Alan Bowling. *Analysis of Robotic Manipulator Dynamic Performance: Acceleration and Force Capabilities.* PhD thesis, Stanford University, June 1998.

[3] Alan Bowling and Oussama Khatib. Analysis of the acceleration characteristics of manipulators. In A. Morecki, G. Bianchi, and K. Jaworek, editors, *Proceedings Tenth CISM-IFToMM Symposium on Theory and Practice of Robots and Manipulators (Romansy 10)*, pages 59–64. Springer-Verlag, September 1995. Gdansk, Poland.

[4] Alan Bowling and Oussama Khatib. Analysis of the acceleration characteristics of non-redundant manipulators. In *Proceedings IEEE/RSJ International Conference on Intelligent Robots and Systems*, volume 2, pages 323–328. IEEE Computer Society Press, August 1995. Pittsburgh, Pennsylvania.

[5] Timothy J. Graettinger and Bruce H. Krogh. The acceleration radius: A global performance measure for robotic manipulators. *IEEE Journal of Robotics and Automation*, 4(1), February 1988.

[6] Oussama Khatib. Inertial properties in robotic manipulation: An object-level framework. *The International Journal of Robotics Research*, 13(1):19–36, February 1995.

[7] Oussama Khatib and Joel Burdick. Optimization of dynamics in manipulator design: The operational space formulation. *The International Journal of Robotics and Automation*, 2(2):90–98, 1987.

[8] Yong-Yil Kim and Subhas Desa. The definition, determination, and characterization of acceleration sets for spatial manipulators. In *The 21st Biennial Mechanisms Conference: Flexible Mechanism, Dynamics, and Robot Trajectories*, September 1990. Chicago, Illinois.

[9] Yong-Yil Kim and Subhas Desa. The definition, determination, and characterization of acceleration sets for planar manipulators. In *The 21st Biennial Mechanisms Conference: Flexible Mechanism, Dynamics, and Robot Trajectories*, September 1990. Chicago, Illinois.

[10] Charles A. Klein and Bruce E. Blaho. Dexterity measures for the design and control of kinematically redundant manipulators. *The International Journal of Robotics Research*, 6(2):72–83, 1987.

[11] Kazuhiro Kosuge and Katsuhisa Furuta. Kinematic and dynamic analysis of robot arm. In *Proceedings IEEE International Conference on Robotics and Automation*, volume 2, 1985.

[12] Ou Ma and Jorge Angeles. The concept of dynamic isotropy and its applications to inverse kinematics and trajectory planning. In *Proceedings IEEE International Conference on Robotics and Automation*, volume 1, 1990.

[13] Ricardo Matone and Bernard Roth. Designing manipulators for both kinematic and dynamic isotropy. In A. Morecki, G. Bianchi, and C. Rzymkowski, editors, *Proceedings Tenth CISM-IFToMM Symposium on Theory and Practice of Robots and Manipulators (Romansy 11)*, 1997.

[14] Ricardo Matone and Bernard Roth. The effects of actuation schemes on the kinematic performance of manipulators. *Journal of Mechanical Design, Transactions ASME*, 119, 1997.

[15] R. V. Mayorga, B. Ressa, and A. K. C. Wong. A dexterity measure for robot manipulators. In *Proceedings IEEE International Conference on Robotics and Automation*, volume 1, 1990.

[16] J. Kenneth Salisbury and John J. Craig. Articulated hands: Force control and kinematic issues. *The International Journal of Robotics Research*, 1(1):4–17, 1982.

[17] M. Thomas, H. C. Yuan-Chou, and D. Tesar. Optimal actuator sizing for robotic manipulators based on local dynamic criteria. *Transactions of the ASME Journal of Mechanisms, Transmissions, and Automation in Design*, 107(2):163–169, 1985.

[18] Masaru Uchiyama, Kunitoshi Shimizu, and Kyojiro Hakomori. Performance evaluation of manipulators using the jacobian and its application to trajectory planning. In *Robotics Research, The Second International Symposium*, 1985.

[19] Tsuneo Yoshikawa. Dynamic manipulability of robot manipulators. In *Proceedings 1985 IEEE International Conference on Robotics and Automation*, pages 1033–1038, 1985. St. Louis, Missouri.

[20] Tsuneo Yoshikawa. Manipulability of robotic mechanisms. *The International Journal of Robotics Research*, 4(2), 1985.

[21] Tsuneo Yoshikawa. Translational and rotational manipulability of robotic manipulators. In *Proceedings of the 1991 International Conference Industrial Electronics, Control, and Instrumentation*, October 1991.

[22] Zhanfang Zhao, Zhen Wu, Jilian Lu, Weihai Chen, and Guanghua Zong. Dynamic dexterity of redundant manipulators. In *Proceedings IEEE International Conference on Robotics and Automation*, volume 2, 1995.